ChemComm

COMMUNICATION

View Article Online
View Journal | View Issue

Cite this: *Chem. Commun.*, 2018, **54**, 2425

Received 22nd December 2017,
Accepted 12th February 2018

DOI: 10.1039/c7cc09765d

rsc.li/chemcomm

Gadolinium based endohedral metallofullerene $Gd_2@C_{79}N$ as a relaxation boosting agent for dissolution DNP at high fields†

Xiaoling Wang, ‡*[a] Johannes E. McKay,‡[a] Bimala Lama,[b] Johan van Tol,[a] Tinghui Li,[c] Kyle Kirkpatrick,[c] Zhehong Gan,[a] Stephen Hill,[ad] Joanna R. Long[b] and Harry C. Dorn[c]

We show increased dynamic nuclear polarization by adding a low dosage of a S = 15/2 Gd based endohedral metallofullerene (EMF) to DNP samples. By adding 60 μM $Gd_2@C_{79}N$, the nuclear polarization of ^{1}H and ^{13}C spins from 40 mM 4-oxo-TEMPO increases by approximately 40% and 50%, respectively, at 5 T and 1.2 K. Electron–electron double resonance (ELDOR) measurements show that the high spin EMF shortens the electron relaxation times and increases electron spectral diffusion leading to the increased DNP enhancement.

Dynamic nuclear polarization (DNP) has gained popularity in recent years as an effective method to address the nuclear spin sensitivity challenges of NMR and MRI. In particular, by combining DNP at low temperature with rapid dissolution, nuclear spin polarization enhancements on the order of 10 000 fold over thermal equilibrium can be achieved for room temperature solutions, enabling novel applications monitoring *in vivo* metabolism in real time.[1,2] The use of Gd^{3+} reagents, such as $GdCl_3$ or Gd-chelates, co-dissolved at millimolar concentrations with stable organic radicals, such as the trityl radical OX063, has previously been shown to increase nuclear hyperpolarization at low temperatures.[3] Adding millimolar Gd-chelates can yield an up to 250% increase in ^{13}C polarization at 3.35 T for various dissolution DNP formulations incorporating OX063.[3–5] The increased DNP enhancement has been attributed to a shortening of the electron relaxation time T_{1e} toward an optimum for the thermal mixing DNP mechanism.[3] Pursuing dissolution-DNP at higher magnetic fields would enable further benefits from increased electron polarization.[2,6] However, moving DNP experiments to higher magnetic fields brings a counter-acting challenge; a significantly slower buildup of ^{13}C polarization is seen at 4.6 T,[7] and this buildup time becomes the primary constraint for experiments at higher fields. Due to faster ^{1}H polarization build up times, ^{1}H DNP followed by cross polarization to ^{13}C spins has an advantage over direct ^{13}C DNP[8,9] to boost dissolution DNP efficiency. As an accessible and inexpensive alternative to the OX063 radical, TEMPO has been demonstrated for direct DNP enhancements at w-band (94 GHz/3.35 T) and higher fields.[10–12] This raises the possibility that adding a relaxation boosting agent to DNP samples, using the TEMPO radical for high field dissolution DNP, could similarly dramatically increase DNP enhancements, with faster buildup times for both indirect, *via* ^{1}H–^{13}C cross polarization, and direct ^{13}C polarization approaches. However, for DNP samples containing either trityl or TEMPO at higher magnetic field strengths (above 3.35 T), the beneficiary effects of Gd compounds has rarely been reported. At fields of 4.6 T[7] and 7 T,[13] either very slight improvements or slight decreases in polarization have been observed for ^{13}C spins in samples containing both Gd-chelates and OX063. In samples containing TEMPO, addition of 2 mM Gd-chelates slightly decreased ^{13}C polarization at 5 T.[12] Therefore, for high-field DNP applications beyond w-band, alternative Gd-based compounds that can show positive effects on DNP are in demand. In contrast to Gd-chelates that have been reported in DNP studies so far, at higher magnetic fields, such compounds should be able to effectively influence TEMPO electron relaxation times and produce an optimal electron polarization profile for achieving increased nuclear hyperpolarizations.

In this study we present the novel application of a gadolinium-based endohedral metallofullerene[14] (EMF), $Gd_2@C_{79}N$,[15] which can effectively enhance ^{1}H and ^{13}C nuclear hyper-polarization at field strengths up to 5 T in samples utilizing 4-oxo-TEMPO as the polarizing radical. $Gd_2@C_{79}N$ has a ferromagnetic high-spin ground state of S = 15/2 arising from strong exchange coupling between the two S = 7/2 encapsulated Gd(III) atoms and the S = 1/2 radical associated with the heterofullerene cage $(C_{79}N)^{6-}$, as observed by EPR[15] and estimated by computational studies.[16,17] This strong exchange interaction has resulted in some $Ln_2@C_{79}N$

[a] *National High Magnetic Field Laboratory, Tallahassee, FL 32310, USA. E-mail: xiaoling.wang@magnet.fsu.edu*
[b] *Department of Biochemistry and Molecular Biology, University of Florida, Gainesville, FL 32603, USA*
[c] *Department of Chemistry, Virginia Tech, Blacksburg, VA 24061, USA*
[d] *Department of Physics, Florida State University, Tallahassee, FL 32306, USA*

† Electronic supplementary information (ESI) available: Simulated ELDOR spectra and decay curve of hyperpolarized proton signal. See DOI: 10.1039/c7cc09765d

‡ These authors contributed equally to this work.

(and related; Ln = lanthanide) EMFs displaying novel magnetic properties, including single-molecule magnet behavior.[16–20] Thus, $Gd_2@C_{79}N$ is an attractive target as an efficient relaxation agent for boosting DNP enhancements due to its high spin ground state. It is also advantageous that Gd-based EMFs are already known for their use as MRI contrast agents for *in vivo* imaging, having superior clinical compatibility as they require significantly lower dosages for measurable contrast compared with Gd-chelates; the latter are known to aggregate in aqueous environments, thus reducing their efficacy. Here we report the positive impact of $Gd_2@C_{79}N$ as a relaxation enhancing agent for dissolution-DNP experiments at high fields, using 30 times lower concentration compared to previous reports for Gd-chelates. Pulsed EPR experiments measuring electron spin relaxation and spectral diffusion, described below, explain the mechanism for the DNP improvements seen upon addition of $Gd_2@C_{79}N$.

The electron longitudinal relaxation time, T_{1e}, of radical polarizing agents is a critical factor determining DNP efficiency. At temperatures typical for dissolution DNP (1–2 K), T_{1e} is usually very long for radicals (typically 500 ms for TEMPO at 1.5 K); the addition of a fast relaxing high-spin species, such as $Gd_2@C_{79}N$, increases the relaxation rate for the slowly relaxing spin species, *i.e.*, TEMPO in the present case. Because of the fullerene encapsulation, the coupling of $Gd_2@C_{79}N$ to TEMPO is through dipolar interactions rather than exchange. Since the dipolar coupling strength scales with the factor $S(S + 1)$, it is readily apparent that an increase in spin quantum number from 7/2 to 15/2 increases the effectiveness of the Gd^{3+} EMF for reducing the T_{1e} of the TEMPO radical by a factor of 4.6. In addition, the fact that the $Gd_2@C_{79}N$ molecules disperse uniformly in toluene glass at cryogenic temperatures further improves its efficacy as an electron relaxation agent in comparison to Gd-chelates.

Electron relaxation measurements were performed at 3.35 T, a field close to that of the DNP polarizer. Table 1 shows the effect of 60 μM $Gd_2@C_{79}N$ on the 4-oxo-TEMPO T_{1e} and T_M, the spin echo decay time constant. The electron T_{1e}, which was measured using a saturation recovery pulse sequence, indicates an approximately eightfold reduction (45 to 5.7 ms) upon addition of $Gd_2@C_{79}N$ (Fig. 1). However, even when using long saturation pulses (longer than T_{1e}), it is expected that there will be a significant spectral diffusion component which is difficult to separate from the longer intrinsic electron T_{1e} relaxation, even when fitting to a bi-exponential decay function. Therefore, the observed decrease in T_{1e} is likely due to a combination of

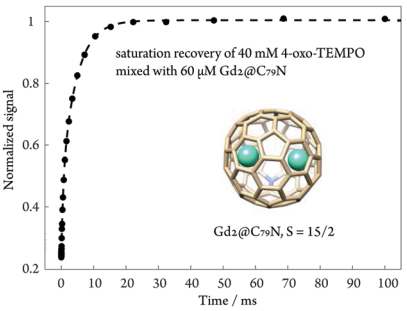

Fig. 1 Molecular structure of $Gd_2@C_{79}N$ and T_{1e} saturation recovery curve of 40 mM 4-oxo-TEMPO with 60 μM $Gd_2@C_{79}N$ measured at 3.35 T and 6.5 K. Saturation pulse length of 300 ms was used.

the two mechanisms. The 4-oxo-TEMPO T_M measured by the Hahn echo pulse sequence indicates an approximately 1.8 fold reduction (920 to 520 ns) upon addition of $Gd_2@C_{79}N$ (Fig. S3, ESI†). Again, this can in part be explained by the dipolar coupling between the S = 15/2 spin and the S = 1/2 radical, which enhances spin decoherence.

For polarizing agents such as 4-oxo-TEMPO that exhibit significant inhomogeneous broadening of their EPR spectra due to large g-tensor anisotropy, electron spectral diffusion (eSD) influences the polarization profile across the EPR spectrum and, hence, the efficiency of DNP.[10,21–23] Electron–electron double resonance (ELDOR) experiments were thus performed to probe the influence of $Gd_2@C_{79}N$ on the 4-oxo-TEMPO eSD processes. W-band measurements were carried out using a high power (1 kW) quasi-optical 94 GHz spectrometer (HiPER),[24] taking advantage of its wide-band double resonance capability for pulsed studies of broad EPR spectra. The experiments involve applying a long (ms duration) variable-frequency saturation pulse (Rabi frequency Ω_R = 0.2 MHz), followed by a fixed-frequency echo-detection sequence. The experiment probes eSD by monitoring changes in electron polarization at one location in the 4-oxo-TEMPO EPR spectrum, set by the echo-detection frequency, brought about *via* saturation (depolarization) at a different position within the spectrum. ELDOR spectra (Fig. 2) are plotted as a function of the detuning, $\delta\nu$, from the maximum of the echo-detected EPR spectrum; the saturation pulse frequency is then stepped across the entire EPR spectrum, while the detection frequency is fixed. The sharp drops in polarization occur when the saturation and detection frequencies coincide, and at sidebands corresponding to zero- and double-quantum transitions associated with hyperfine coupling of the radical to ^{1}H and ^{13}C nuclear spins. Meanwhile, the broad background is indicative of the eSD.

ELDOR data for the 4-oxo-TEMPO radical with and without the $Gd_2@C_{79}N$ relaxation agent, were fit to a model developed by Vega *et al.*[22] for DNP samples containing relatively high electron spin concentrations. The model derives the electron spin polarization profiles across the EPR spectrum using a set of rate equations, accounting for microwave-induced electron and nuclear spin transitions, electron and nuclear relaxation, nuclear spin diffusion and the eSD mechanism. The eSD rate, $\bar{w}_{j,j'}$, in the model describes the polarization exchange between pairs of electron spins, which depends on their frequency

Table 1 Experimentally measured electron relaxation times for 40 mM 4-oxo-TEMPO in toluene (exp. T_{1e}, exp. T_M) and parameters (par. T_{1e}, par. T_{2e}) used for the best fit simulations of ELDOR spectra at 3.35 T and 6.5 K. Λ^{eSD} represents the electron polarization exchange rate of the eSD process, and $\bar{A}^{\pm}_{1H}$ and $\bar{A}^{\pm}_{13C}$ measure the hyperfine coupling strength between nuclei and electrons

$Gd_2@C_{79}N$ conc./μM	Exp. T_{1e}/ms	Exp. T_M/ns	Par. T_{1e}/ms	Par. T_{2e}/μs	Λ^{eSD}/ $\times 10^{-6}$ s^{-3}	$\bar{A}^{\pm}_{1H}$/ MHz	$\bar{A}^{\pm}_{13C}$/ MHz
0	45	920	45	10	180 ± 10	4 ± 0.5	0.9 ± 0.1
60	5.7	520	15	10	350 ± 20	7 ± 1.0	1.8 ± 0.2

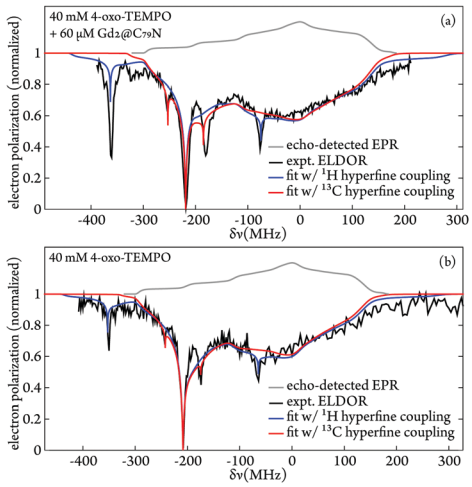

Fig. 2 Experimental ELDOR spectra and fits both with (a) and without (b) the $Gd_2@C_{79}N$ relaxation agent. The fits were performed using the model described in ref. 22 that considers hyperfine coupling with ^1H and ^{13}C nuclear spins. The saturation pulse frequency was swept over a 600 MHz bandwidth (1 MHz steps), followed by Hahn-echo detection sequence at $\delta\nu = -219$ MHz in (a) and -209 MHz in (b). Electron depolarization by solid effect (SE) polarization transfer is seen at two positions, detuned approximately ± 36 MHz and ± 143 MHz from the detection frequencies, resulting from hyperfine interactions with the ^{13}C (67% isotope enriched) and ^1H nuclei. The fit parameters are given in Table 1. Other parameters: saturation pulse length of 23 ms.

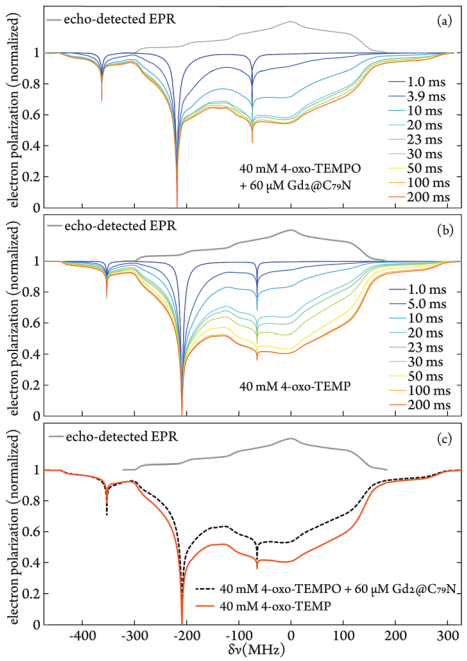

Fig. 3 Simulated ELDOR spectra as a function of the saturation pulse length, both with (a) and without (b) the $Gd_2@C_{79}N$ relaxation agent. (c) Superimposed simulations of the ELDOR spectra for both samples for a saturation pulse length of 200 ms. The simulations assume hyperfine coupling to ^1H spins. The simulations assume hyperfine coupling to ^1H nuclear spins. (a and b) used the respective experimental detection frequencies employed in Fig. 2, while (c) used the same value of $\delta\nu = -209$ MHz for both samples.

difference $(\omega_j - \omega_{j'})$ through the simplified expression of eqn (1), which assumes a Lorenzian line-shape;[22] the lone fit parameter Λ^{eSD} is given in Table 1. ELDOR simulations in Fig. 3 show the dependence of the electron spin polarization profiles on the saturation pulse length. As shown in Fig. S4 (ESI†), good agreement is obtained in terms of the saturation pulse length employed for the ELDOR measurements in Fig. 2. The fits indicate that addition of $Gd_2@C_{79}N$ shortens the intrinsic 4-oxo-TEMPO electron T_{1e} from 45 to 15 ms. The simulations in Fig. 3(c) show that, using a long saturation pulse of 200 ms, the ELDOR spectrum of 4-oxo-TEMPO with $Gd_2@C_{79}N$ is narrower than the one without it. The differences in the ELDOR spectra, and hence the electron polarization profiles, should be a consequence of both the shortening of T_{1e} and an increase in the eSD rate from 180 to 350 $\times$ 10^{-6} s^{-3}. The eSD rate has previously been suggested to play a significant role in the observed increase in DNP enhancements upon addition of Gd-chelates.[25] The increase in spectral diffusion is also consistent with the drastic shortening of the experimental T_{1e} measured *via* saturation recovery upon addition of $Gd_2@C_{79}N$.

$$\overline{w}^{eSD}_{j,j'} = \frac{\Lambda^{eSD}}{(\omega_j - \omega_{j'})^2} \quad (1)$$

The DNP enhancement observed using 40 mM 4-oxo-TEMPO at 5 T and 1.2 K is predominantly due to nuclear spin flips concerted with flip-flops of pairs of coupled electron spins whose Zeeman energies differ by the nuclear Larmor frequency. The nuclear polarization is correlated to the polarization difference of the electron spin pairs, and this difference is generated by direct microwave irradiation in the case of the cross effect (CE). With the sample system and experimental conditions described in this work, the polarization difference is also governed by indirect depolarization *via* eSD and T_{1e} relaxation, a DNP mechanism termed the indirect cross effect (iCE).[21,25] In the process of iCE, the electron polarization exchange mediated by eSD can indirectly depolarize one of the transitions of CE electron spin pairs that cannot be directly saturated by microwave irradiation. Consequently, changes of the polarization difference of those CE electron spin pairs can cause changes of nuclear spin polarization, leading to DNP enhancements.

For radicals such as 4-oxo-TEMPO that have inhomogeneously broadened EPR spectra, low power microwave irradiation only saturates transitions that are "on-resonance", burning a hole in the EPR spectrum. Without eSD, microwave irradiation only generates a polarization gradient near the excitation frequency rather than across the entire EPR lineshape. The eSD process, mediated by flip-flops among coupled electron spins, is much faster than T_{1e}. Thus, spectral diffusion away from the saturated region can rapidly spread depolarization across the EPR line profile. For samples with very long T_{1e}, on-resonant saturation and rapid spectral diffusion can lead to a partial saturation of the entire EPR spectrum. This broad saturation reduces the spectral polarization gradient and, therefore, has a negative impact on DNP enhancement. However, shortening T_{1e} will reduce this saturation, thereby maintaining a

Table 2 ^{1}H DNP enhancement factors, decay time constants of hyperpolarized ^{1}H NMR signal, and ^{13}C DNP enhancement factors of toluene containing 40 mM 4-oxo-TEMPO at 5 T and 1.2 K.[26] Continuous MW irradiation at 140.71 GHz was used to create DNP polarization at the positive maximum enhancement of the DNP profiles for 4-oxo-TEMPO. The maximum enhancement frequency does not change upon the addition of $Gd_2@C_{79}N$ (see ESI for other experiment parameters)

$Gd_2@C_{79}N$ conc./μM	^{1}H ε	^{1}H t_{decay}/s	^{13}C ε
0	66 ± 7	1330 ± 100	28 ± 6
60	91 ± 9	770 ± 70	43 ± 9

polarization gradient that is more optimal for DNP enhancement. In this study, DNP induced polarization of ^{1}H and ^{13}C spins in toluene containing 60 M $Gd_2@C_{79}N$ and 40 mM 4-oxo-TEMPO increased by approximately 40% and 50%, respectively, relative to a toluene sample containing only 40 mM 4-oxo-TEMPO (Table 2). This is because $Gd_2@C_{79}N$ significantly decreases the 4-oxo-TEMPO T_{1e} due to its large S = 15/2 spin, as confirmed by both electron spin relaxation and ELDOR measurements. In this case, a shorter T_{1e} results in a transformation of the electron polarization gradient, as shown in Fig. 3(c), towards one that is favorable for a greater contribute from the iCE mechanism, which leads to an increase of DNP enhancement. Previous reports of the influence of Gd^{3+} doping on ^{13}C DNP enhancements show that, at a magnetic field strength of 3.35 T, adding 1–8 mM Gd-HP-DO3A results in a maximal 20% increase in the enhancement, and a negligible change in DNP build-up time for samples using TEMPO radicals as the source of electron polarization;[4] at 5 T, the addition of Gd^{3+} even causes a decrease in ^{13}C polarization.[12] In this study, we report significant ^{1}H and ^{13}C DNP enhancement increases at 5 T *via* Gd^{3+} for the first time by using $Gd_2@C_{79}N$ in combination with 4-oxo-TEMPO. The observed polarization boosting effects can benefit both samples suitable for direct ^{13}C polarization and those where ^{1}H–^{13}C cross-polarization transfer can provide experimental advantages.

This work is particularly significant considering the effects of $Gd_2@C_{79}N$ were observed for a 60 μM concentration, whilst millimolar concentrations are required for other Gd^{3+} compounds in order to show any noticeable effect on the electron T_{1e} of the polarizing agent. In fact, Gd^{3+} EMFs enable up to 50 times higher proton relaxivity[27,28] in comparison to conventional Gd-based MRI contrast agents of chelate/macrocyclic structures. Additionally, the encapsulation also provides an inherent advantage of preventing the release of toxic Gd^{3+} ions in medical applications. Future work is proposed to explore the possibility of using these water soluble Gd based EMFs as dual agents for *in vivo* hyperpolarized MRI at various magnetic fields, and the dependence on the doping concentration of Gd based EMFs.

This project was supported by the National Science Foundation (DMR-1610226) and the National Science Foundation Cooperative Agreement (DMR-1157490) and the State of Florida. The authors are grateful to Professor Shimon Vega for the ELDOR simulation program. Professor Songi Han, Alisa Leavesley, and Frederic Mentink are warmly acknowledged for insightful discussions.

Conflicts of interest

There are no conflicts to declare.

References

1 J. H. Ardenkjaer-Larsen, B. Fridlund, A. Gram, G. Hansson, L. Hansson, M. H. Lerche, R. Servin, M. Thaning and K. Golman, *Proc. Natl. Acad. Sci. U. S. A.*, 2003, **100**, 10158–10163.
2 J. H. Ardenkjaer-Larsen, *J. Magn. Reson.*, 2016, **264**, 3–12.
3 H. J. Ardenkjaer-Larsen, S. Macholl and H. Jóhannesson, *Appl. Magn. Reson.*, 2008, **34**, 509–522.
4 L. Lumata, M. E. Merritt, C. R. Malloy, A. D. Sherry and Z. Kovacs, *J. Phys. Chem. A*, 2012, **116**, 5129–5138.
5 A. Flori, M. Liserani, S. Bowen, J. H. Ardenkjaer-Larsen and L. Menichetti, *J. Phys. Chem. A*, 2015, **119**, 1885–1893.
6 F. Jähnig, G. Kwiatkowski and M. Ernst, *J. Magn. Reson.*, 2016, **264**, 22–29.
7 H. Jóhannesson, S. Macholl and J. H. Ardenkjaer-Larsen, *J. Magn. Reson.*, 2009, **197**, 167–175.
8 S. Jannin, A. Bornet, S. Colombo and G. Bodenhausen, *Chem. Phys. Lett.*, 2011, **517**, 234–236.
9 S. Jannin, A. Bornet, R. Melzi and G. Bodenhausen, *Chem. Phys. Lett.*, 2012, **549**, 99–102.
10 T. A. Siaw, M. Fehr, A. Lund, A. Latimer, S. A. Walker, D. T. Edwards and S.-I. Han, *Phys. Chem. Chem. Phys.*, 2014, **16**, 18694–18706.
11 L. L. Lumata, R. Martin, A. K. Jindal, Z. Kovacs, M. S. Conradi and M. E. Merritt, *Magn. Reson. Mater. Phys., Biol. Med.*, 2015, **28**, 195–205.
12 A. Kiswandhi, B. Lama, P. Niedbalski, M. Goderya, J. Long and L. Lumata, *RSC Adv.*, 2016, **6**, 38855–38860.
13 S. A. Walker, D. T. Edwards, T. A. Siaw, B. D. Armstrong and S. Han, *Phys. Chem. Chem. Phys.*, 2013, **15**, 15106–15120.
14 J. R. Heath, S. C. O'Brien, Q. Zhang, Y. Liu, R. F. Curl, F. K. Tittel and R. E. Smalley, *J. Am. Chem. Soc.*, 1985, **107**, 7779–7780.
15 W. Fu, J. Zhang, T. Fuhrer, H. Champion, K. Furukawa, T. Kato, J. E. Mahaney, B. G. Burke, K. A. Williams, K. Walker, C. Dixon, J. Ge, C. Shu, K. Harich and H. C. Dorn, *J. Am. Chem. Soc.*, 2011, **133**, 9741–9750.
16 F. Cimpoesu, B. Frecus, C. I. Oprea, H. Ramanantoanina, W. Urland and C. Daul, *Mol. Phys.*, 2015, **113**, 1712–1727.
17 M. K. Singh, N. Yadav and G. Rajaraman, *Chem. Commun.*, 2015, **51**, 17732–17735.
18 R. Westerström, J. Dreiser, C. Piamonteze, M. Muntwiler, S. Weyeneth, H. Brune, S. Rusponi, F. Nolting, A. Popov, S. Yang, L. Dunsch and T. Greber, *J. Am. Chem. Soc.*, 2012, **134**, 9840–9843.
19 F. Liu, D. S. Krylov, L. Spree, S. M. Avdoshenko, N. A. Samoylova, M. Rosenkranz, A. Kostanyan, T. Greber, A. U. B. Wolter, B. Büchner and A. A. Popov, *Nat. Commun.*, 2017, **8**, 16098.
20 Z. Hu, B.-W. Dong, Z. Liu, J.-J. Liu, J. Su, C. Yu, J. Xiong, D.-E. Shi, Y. Wang, B.-W. Wang, A. Ardavan, Z. Shi, S.-D. Jiang and S. Gao, *J. Am. Chem. Soc.*, 2018, **140**, 1123–1130.
21 Y. Hovav, D. Shimon, I. Kaminker, A. Feintuch, D. Goldfarb and S. Vega, *Phys. Chem. Chem. Phys.*, 2015, **17**, 6053–6065.
22 Y. Hovav, I. Kaminker, D. Shimon, A. Feintuch, D. Goldfarb and S. Vega, *Phys. Chem. Chem. Phys.*, 2015, **17**, 226–244.
23 W. Wenckebach, *J. Magn. Reson.*, 2017, **277**, 68–78.
24 P. A. S. Cruickshank, D. R. Bolton, D. A. Robertson, R. I. Hunter, R. J. Wylde and G. M. Smith, *Rev. Sci. Instrum.*, 2009, **80**, 103102.
25 E. Ravera, D. Shimon, A. Feintuch, D. Goldfarb, S. Vega, A. Flori, C. Luchinat, L. Menichetti and G. Parigi, *Phys. Chem. Chem. Phys.*, 2015, **17**, 26969–26978.
26 B. Lama, J. H. P. Collins, D. Downes, A. N. Smith and J. R. Long, *NMR Biomed.*, 2016, **29**, 226–231.
27 M. Chaur, F. Melin, A. Ortiz and L. Echegoyen, *Angew. Chem., Int. Ed.*, 2009, **48**, 7514–7538.
28 J. Zhang, P. P. Fatouros, C. Shu, J. Reid, L. S. Owens, T. Cai, H. W. Gibson, G. L. Long, F. D. Corwin, Z.-J. Chen and H. C. Dorn, *Bioconjugate Chem.*, 2010, **21**, 610–615.

